Letters

Transient Stability Analysis of Microgrid Considering Impact of Grid-Following Converter's Current Controller

Yawen Ding, *Student Member, IEEE*, Fei Gao, *Member, IEEE*, and Muhammad Mansoor Khan, *Member, IEEE*

***Abstract*—The dynamics of current controller is usually neglected for simplification when assessing microgrid transient stability. Utilizing the Takagi–Sugeno method, this letter thoroughly examines the effects of current controller on transient stability estimations and reveals that completely ignoring the dynamics of current controller can cause overestimation on transient stability. The findings highlight a significant overestimation on lower boundary of angle about 29.2% even if current controller performs fast dynamics with bandwidth more than 28 times the fundamental frequency. Recognizing the impracticality of including current controller dynamics in microgrids with multiple converters, this letter proposes a stability-enhanced method through phase compensation in the current controller, which can improve the accuracy of transient stability assessments while still omitting current controller dynamics. In addition, a guideline for parameter design of phase compensation is provided. Theoretical findings are verified by hardware-in-loop experimental results based on OPAL-RT platform.**

***Index Terms*—Current controller, grid-following converter (GFLC), islanded microgrid (MG), Takagi—Sugeno (TS) method, transient stability.**

I. Introduction

With the increased penetration of renewable energy resources and power electronic converters [1], microgrid (MG) has been widely adopted owing to high reliability and flexibility [2]. However, the low inertia and high nonlinearity of power electronic converters bring new challenges to the stable operation of MG. Particularly, an islanded MG is easier to become unstable under large disturbances [3].

To tackle the issue, transient stability for the MG have been widely studied in recent years, which can be grouped into three categories: time-domain analysis [4], equal area criterion [5] and Lyapunov-based method [6], [7], [8], [9], [10], [11], [12], [13], [14], [15], [16], [17]. Among these approaches, Lyapunov-based method has become a favorable choice because it can give an insightful view on the instability mechanism and estimate the system's stability region for complicated MG.

The widely used Lyapunov-based methods include Hamiltonian theory [6], mixed potential theory (MPT) [7], sum of squares (SOS) programming [8] and Takagi–Sugeno (TS) multimodeling [9]. Both Hamilton theory and MPT can provide stability criterion in analytic form, but the dynamics of the current controller is assumed to be quite fast to be neglected for transient stability analysis of MG in [10]. Although the authors in [11] and [12] considered dynamics of the current controller when assessing transient stability of MG, the results are still untrustworthy because the constructed mixed potential function no longer satisfies the basic conditions of MPT, i.e., the differential relation with voltages across the capacitors. SOS programming can estimate domain of attraction (DOA) for MG by solving the optimization problem and comprehensively reflect the influence of all controllers in the MG, but the influence of current controller on the system's transient stability is still not revealed in [13]. Moreover, the increased computation time due to the order of constructed Lyapunov function makes it ill-suited for on-line stability analysis. TS multimodeling describes a nonlinear MG by a sum of linear models, so the stability can be analyzed by methodologies intend for linear systems. Although the increase of nonlinearities leads to the exponential increased computation for TS method, some efforts have been made to extend its application for large-scale MG, such as model reduction [14] and dividing MG into interconnected dissipative subsystems [15]. Hence, TS method becomes more suitable for transient stability analysis of complicated MGs. The DOA of MG is estimated by the TS method in [16], but the estimation does not consider the dynamics of voltage and current controller. In [17], the TS multimodeling of the MG including circuits and controllers is established. The effect of circuit parameters on the DOA of the MG is analyzed while the impact of current controller on the transient stability of the MG is still not quantified.

In the existing literatures, whether ignoring the dynamics of the current controller will lead to misleading result of transient stability is still unknown. Thus, this letter investigates the impact of current controller on the transient stability of MG and the accuracy of transient stability assessment ignoring dynamics of

Manuscript received 15 February 2024; revised 10 April 2024; accepted 28 April 2024. Date of publication 1 May 2024; date of current version 20 June 2024. This work was supported by the Science and Technology Project of Headquarters of State Grid Corporation of China under Grant 5108-202218280A-2-69-XG. *(Corresponding author: Fei Gao.)*

Yawen Ding is with the College of Smart Energy, Shanghai Jiao Tong University, Shanghai 200240, China (e-mail: dingyawen@sjtu.edu.cn).

Fei Gao and Muhammad Mansoor Khan are with the Key Laboratory of Control of Power Transmission and Conversion, Ministry of Education, Department of Electrical Engineering, Shanghai Jiao Tong University, Shanghai 200240, China (e-mail: fei.gao@sjtu.edu.cn; mansoor@sjtu.edu.cn).

Color versions of one or more figures in this article are available at https://doi.org/10.1109/TPEL.2024.3395839.

Digital Object Identifier 10.1109/TPEL.2024.3395839

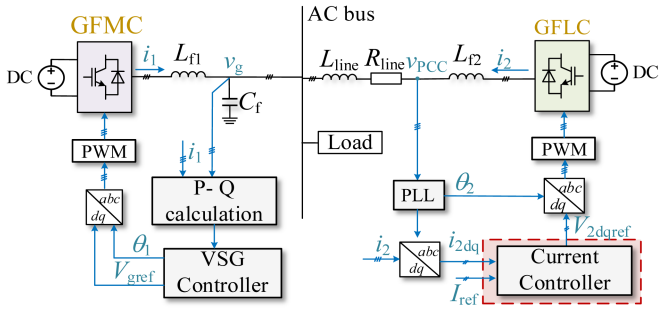

Fig. 1. Islanded MG under study.

current controller. In addition, a phase compensation term is added in the current controller to improve the transient stability of the MG.

II. Dynamic Modeling of the MG

Fig. 1 depicts the studied MG containing a grid-following converter (GFLC), a grid-forming converter (GFMC) and a resistive load R_{load}. C_f and L_{f1} represents the filter capacitance and inductance of GFMC, respectively. L_{f2} represents the filter inductance of GFLC. L_{line} and R_{line} represent cable inductance and resistance of GFLC, respectively.

The GFMC is controlled as virtual synchronous generator to provide voltage and frequency support for the MG while the GFLC are regulated by the conventional phase-locked loop (PLL) and PI-based current controller. GFMC and GFLC are working in axis d_1–q_1 and axis d_2–q_2 frames rotating at frequency of ω_1 and ω_2, respectively, and the angle difference δ_{21} between GFLC and GFMC can be expressed as

$$\delta_{21} = \theta_2 - \theta_1, \dot{\delta}_{21} = \omega_2 - \omega_1. \tag{1}$$

A. Dynamic Model Ignoring Current Controller

The dynamics of voltage and frequency provided by GFMC for ac bus can be expressed as

$$K_1 \dot{v}_{gd} = Q_0 - Q_1 - D_{q1}(v_{gd} - E_0) \tag{2}$$

$$J_1 \dot{\omega}_1 = P_0/\omega_0 - K_{p1}(\omega_1 - \omega_0) - P_1/\omega_0 - D_{p1}\omega_1 \tag{3}$$

where E_0 and ω_0 are the reference voltage and angular frequency of GFMC. K_1 and D_{q1} are the voltage integral coefficient and Q-V coefficient of GFMC, respectively. P_0 and Q_0 are the reference powers of GFMC, P_1 and Q_1 are the actual output powers of GFMC. J_1 and D_{p1} are the inertia constant and damping coefficient, respectively. K_{p1} is the parameter of speed governor. Assuming that GFMC operates under unity power factor, P_1 and Q_1 can be calculated as

$$\begin{aligned} P_1 &= 1.5(v_{gd}/R_{\text{load}} - \cos\delta_{21} i_{2d} + \sin\delta_{21} i_{2q}) v_{gd} \\ Q_1 &= 1.5(\sin\delta_{21} i_{2d} + \cos\delta_{21} i_{2q}) v_{gd} \end{aligned} \tag{4}$$

where i_{1d} and i_{1q} are output current of GFMC in axis d_1–q_1, respectively. i_{2d} and i_{2q} are output current of GFLC in axis d_2–q_2, respectively. v_{gd} is the voltage of GFMC in axis d_1.

The dynamic of angular frequency for GFLC is

$$\dot{\omega}_2 = K_p \dot{v}_{\text{PCC}q} + K_i v_{\text{PCC}q} \tag{5}$$

where K_P and K_i are PI parameters of the PLL and they are designed based on damping ratio and settling time of PLL [18]. $v_{\text{PCC}q}$ is the PCC voltage in axis q_2, which can be expressed as

$$v_{\text{PCC}q} = -\sin\delta_{21} v_{gd} + \omega_2 L_{\text{line}} i_{2d} + R_{\text{line}} i_{2q} + L_{\text{line}} \dot{i}_{2q}. \tag{6}$$

In [5] and [10], the dynamics of current controller for GFLC is ignored by assuming the dynamic of current controller is much faster than that of PLL. Hence, i_{2d} and i_{2q} are equal to steady states, i.e., $i_{2d} = I_{d\text{ref}}$ and $i_{2q} = 0$.

Combining (1)–(6), the dynamics of the MG ignoring current controller is a fourth order nonlinear state space model with state variables δ_{21}, ω_1, ω_2, and v_{gd}. For the convenience of transient stability, MG should be transformed to an autonomous system with zero equilibrium points. Hence, the fourth order model can be expressed as $\dot{x} = A(x)x$ with

$$\begin{cases} x_1 = \delta_{12} - \delta_{120}, x_2 = \omega_1 - \omega_{10} \\ x_3 = \omega_2 - \omega_{20}, x_4 = v_{gd} - v_{gd0} \end{cases} \tag{7}$$

$$A = \begin{bmatrix} 0 & -1 & 1 & 0 \\ \frac{-3I_{d\text{ref}} f_2 \sin\delta_{210}}{2J_1\omega_0} & \frac{-K_{p1}-D_{p1}}{J_1} & 0 & A_{24} \\ A_{31} & M_1 K_p f_2 \cos\delta_{210} & A_{33} & A_{34} \\ \frac{-3I_{d\text{ref}} f_2 \cos\delta_{210}}{2K_1} & 0 & 0 & A_{44} \end{bmatrix} \tag{8}$$

$$M_1 = \frac{1}{1 - K_p L_{\text{line}} I_{d\text{ref}}}$$

$$A_{24} = \frac{-3(V_{g1d0}/R_{\text{load}} - I_{d\text{ref}}\cos\delta_{210} + f_2/R_{\text{load}})}{2J_1\omega_0}$$

$$A_{31} = M_1 f_2 \cos\delta_{210} \left(\frac{3K_p I_{d\text{ref}} \sin\delta_{210}}{2K_1} - K_i + \frac{3K_p f_1 I_{d\text{ref}} \cos\delta_{210}}{2K_1} \right)$$

$$A_{33} = M_1(-K_p f_2 \cos\delta_{210} + K_i L_{\text{line}} I_{d\text{ref}})$$

$$A_{34} = M_1 \left(\frac{3K_p I_{d\text{ref}} \sin^2\delta_{210}}{2K_1} - K_i \sin\delta_{210} + \frac{K_p D_{q1} \sin\delta_{210}}{K_1} + \frac{3K_p I_{d\text{ref}} f_1 \sin\delta_{210}\cos\delta_{210}}{2K_1} + \frac{K_p D_{q1} f_1 \cos\delta_{210}}{K_1} \right)$$

$$A_{44} = -\frac{3I_{d\text{ref}} \sin\delta_{210} + 2D_{q1}}{2K_1} \tag{9}$$

where the subscript "0" refers to the steady-state operating point of the MG. A is the nonlinear system matrix containing two nonlinear terms $f_1 = x_1$ and $f_2 = x_4 + v_{gd0}$.

B. Dynamic Model Considering GFLC's Current Controller

To fully reflect the overall dynamics of the MG, the dynamics of current closed-loop including feedforward for decoupling d- and q-axes are considered as follows:

$$\dot{\alpha}_1 = I_{d\text{ref}} - i_{2d}, \dot{\alpha}_2 = -i_{2q}$$

$$(L_{f1} + L_{\text{line}})\dot{i}_{2d} = K_{ip}\dot{\alpha}_1 + K_{ii}\alpha_1 - \cos\delta_{21} v_{gd} - R_{\text{line}} i_{2d}$$

TABLE I
COMPUTATIONAL COMPLEXITY OF TWO MODELS

Model	Model Order	NLT	Number of LMIs
Model without current loop	4th Order	2	2^2+1
Model with current loop	8th Order	5	2^5+1

$$(L_{f1}+L_{\text{line}})\dot{i}_{2q}=K_{ip}\dot{\alpha}_2+K_{ii}\alpha_2+\sin\delta_{21}v_{gd}-R_{\text{line}}i_{2q} \tag{10}$$

where α_1 and α_2 are intermediate variables. K_{iP} and K_{ii} are PI parameters of the current controller, which are design as $K_{ip}=\omega_c\,(L_f+L_{\text{line}})$ and $K_{ii}=\omega_c\,R_{\text{line}}$ so that the current controller can be approximated as a first-order lag system with bandwidth ω_c.

Similarly, the dynamics of the MG considering GFLC's current controller can be formed as a eighth order model with state variables $\delta_{21}, \omega_1, \omega_2, v_{gd}, i_{2\,d}, i_{2\,q}, \alpha_1$, and α_2. The eighth order model can be expressed as $\dot{x}=B(x)x$ with

$$\begin{cases} x_1=\delta_{12}-\delta_{120}, x_2=\omega_1-\omega_{10}, x_3=\omega_2-\omega_{20}, \\ \quad x_4=v_{gd}-v_{gd0} \\ x_5=i_{2d}-i_{2d0}, x_6=i_{2q}-i_{2q0}, x_7=\alpha_1-\alpha_{10}, \\ \quad x_8=\alpha_2-\alpha_{20} \end{cases} \tag{11}$$

where B is the nonlinear system matrix containing five nonlinear terms as follows. For lack of space, B is not shown here

$$\begin{aligned} &g_1=x_1, g_2=\omega_{20}+x_3, g_3=x_4+v_{gd0} \\ &g_4=x_5+I_{\text{dref}}, g_5=x_6. \end{aligned} \tag{12}$$

III. TRANSIENT STABILITY ANALYSIS OF THE MG

In this section, the transient stability of the MG is estimated by means of TS method. The DOAs of dynamic model with and without current controller are compared to investigate the significant influence of neglecting current controller dynamics. Besides, a stability-enhanced method is proposed to compensate the error caused by ignoring current controller.

A. Transient Stability Estimation Based on TS Method

TS method can transform stability analysis of MG into solving linear matrix inequalities (LMI). A MG is asymptotically stable if LMI holds [9]

$$P=P^T>0, PA_i+{A_i}^T P^T<0, i=1,2,\ldots,2^{\text{NLT}} \tag{13}$$

where NLT is the number of nonlinear terms in the system matrix. A_i is the local linear matrix by setting nonlinear terms as the minimum or maximum values. The range of nonlinearities are modified by a small amount to examine the LMI in (13) in each round. Once (13) no longer holds, the maximum estimated DOA can be reached. Since the computation for transient stability estimation depends on the number of LMIs, the computation complexity of dynamics model without current loop and with current loop in Section II is compared in Table I. Despite of 2^5+1 LMI problems in (13) for dynamics considering current loop, the computational complexity is still acceptable.

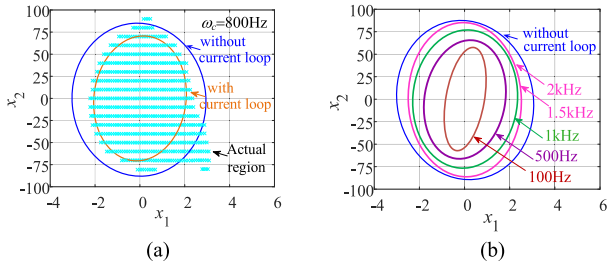

Fig. 2. DOAs of the MG (a) with $\omega_c=800$ Hz and (b) with varying ω_c.

TABLE II
EXPERIMENTAL PARAMETERS

Symbols	Value	Symbols	Value
P_0	20 kW	J_1	15
Q_0	1.5 kVar	D_{p1}	0.01
E_0	311 V	K_1	12
ω_0	314 rad/s	D_{q1}	166.7
K_{p1}	160	L_{line}	15 mH
C_f	1 μF	R_{line}	0.05 Ω
L_{fl}	0.45 mH	K_P	0.56
I_{dref}	15 A	Ki	54
L_{f2}	0.45 mH	R_{load}	8 Ω

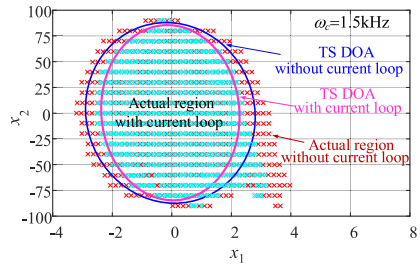

Fig. 3. DOAs of the MG with $\omega_c=1.5$ kHz.

B. Limitation of Neglecting Current Controller's Dynamics

Fig. 2(a) depicts the estimated DOA of MG in Fig. 1 on x_1–x_2 plane with the parameters in Table II where x_1 is δ_{21}–δ_{210} and x_2 is ω_2–ω_{20}. The estimated DOA with current loop and without current loop represents the results of dynamic models in Sections II-A and II-B, respectively.

As seen in Fig. 2(a), the estimated DOA with current loop is inside the actual DOA, which is relatively conservative but sufficient safe for MG's operation. However, the estimated DOA without current loop is larger than the actual DOA, which shows the potential misleading result of neglecting current controller's dynamic for transient stability assessment.

Fig. 2(b) shows the estimated DOAs with different bandwidths of current controller. As ω_c increases from twice fundamental frequency to 20 times fundamental frequency, namely, 100 Hz–2 kHz, the estimated DOA without current loop is always larger than the estimated DOA with current loop. The difference about the stability boundary of x_1 is still distinct even if ω_c is quite high, which means ignoring current controller indeed causes overestimation on transient stability.

To make it clearer for high frequency current loop used in the practical MG, Fig. 3. detailly depicts the DOA of MG with

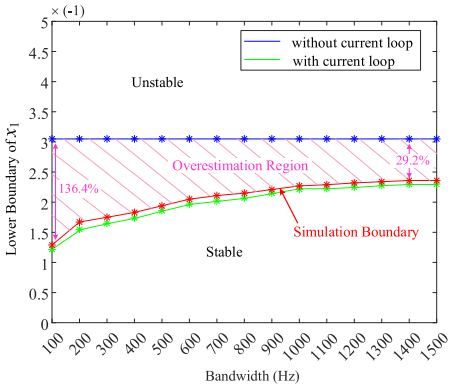

Fig. 4. Stability boundaries for the studied MG.

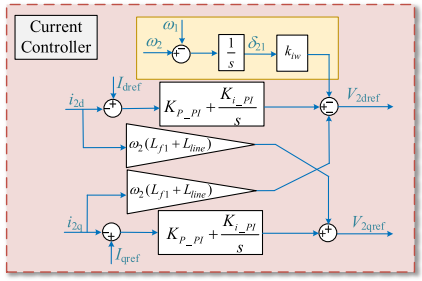

Fig. 5. Block diagram for the proposed stability enhancement method.

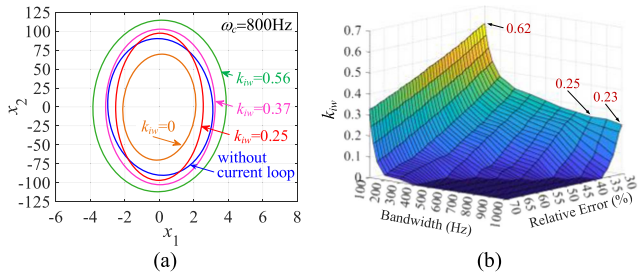

Fig. 6. Results of the proposed method. (a) DOAs of the proposed method. (b) Allowable range for k_{iw}.

$\omega_c = 1.5$ kHz. The comparison of actual DOA and DOA without current loop in Fig. 3 validates the obvious overestimation on lower boundary of x_1 even for high frequency current loop.

To quantify the overestimation on lower boundary of x_1, Fig. 4 shows the relative errors of it between the estimated DOA and actual DOA. The estimated lower boundary of x_1 without current loop is -3.05. The actual lower boundary of x_1 is -1.29 and the relative error reaches 136.4% with $\omega_c = 100$ Hz, which means ignoring current controller with slow dynamics may cause serious overestimation on transient stability. As ω_c increases to 1.4 kHz, the actual lower boundary of x_1 is -2.36 and the relative error is about 29.2%, so ignoring current controller with fast dynamics can still result in erroneous judgement on transient stability. The overestimation remains 29.2% when ω_c is more than 1.4 kHz. Consequently, transient stability assessment by neglecting the dynamics of GFLC's current controller is not valid.

C. Stability-Enhanced Method By Phase Compenstation

In Section III-B, it is seen that transient stability based on dynamics model considering current controller is more trustworthy. However, for the MG equipped with multiple converters, taking dynamics of each converter's current controller into consideration may introduce substantial complexity into the transient stability assessment. Thus, ignoring current controller for multiple converters-based MG when assessing transient stability is unavoidable. To the end, a stability-enhanced method is proposed to enlarge the actual DOA of the MG so as to close the gap between the actual DOA and the estimated DOA without current loop.

Fig. 5 presents a proposed stability-enhanced control scheme where a compensation term is introduced by the phase difference between GFLC and GFMC. The compensation term for the output voltage amplitude of GFLC can be expressed as

$$\Delta V = k_{iw}\frac{\omega_2 - \omega_1}{s} = k_{iw}\delta_{21} \tag{14}$$

where k_{iw} is the proportional gain of the controller.

The proposed method contributes when ω_1 is not equal to ω_2 in transient state. The communication layer is the same as that of distributed secondary control in [19]. Since the compensation term is added to the output of inner current controller, the reference current I_{dref} will not be influenced. Hence, the estimated DOA without current loop remains unchanged while the actual DOA and estimated DOA with current loop will be adjusted.

Fig. 6(a) shows the DOA of the MG with the stability-enhanced control. The estimated DOA with current loop is enlarged with the increase of k_{iw}, which means the transient stability can be enhanced by the proposed method. In particular, setting k_{iw} as 0.25 effectively reduces the difference between the estimated DOA with current loop and the estimated DOA without current loop. However, when k_{iw} increases to 0.37 and 0.56, respectively, the estimated DOA without current loop becomes conservative. Hence, the allowable ranges of k_{iw} need to be found, which provides the design guideline to identify how close the actual stability margin aligns with DOA ignoring current loop's dynamics.

Fig. 6(b) provides the adaptive design of k_{iw} according to the bandwidth of current controller and the relative error of lower boundary of x_1. It can be observed that k_{iw} increases with the decrease of bandwidth and relative error. For instance, when ω_c is 100 and 1000 Hz, respectively, the relative error can be effectively reduced to 30% with $k_{iw} = 0.62$ and $k_{iw} = 0.23$, respectively. When ω_c is set as 800 Hz, the relative error can be reduced to 30% with $k_{iw} = 0.25$, which is consistent with the result in Fig. 6(a).

The phase compensation scheme for MG with N GFLCs and M GFMCs is also preliminarily considered. Since phase differences between converters in the MG remain unchanged at the steady state and frequencies of all converters are the same,

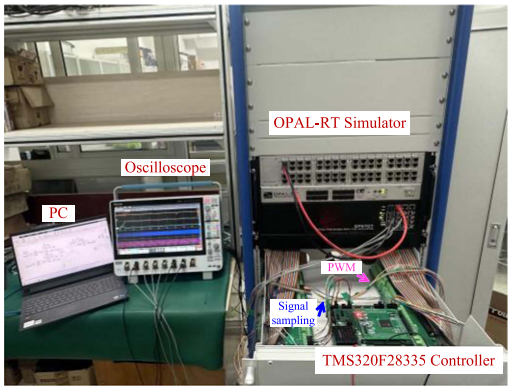

Fig. 7. Experimental setup.

(14) for current controller of GFLC$_i$ can be revised as

$$\omega_{\text{ave}} = \left(\sum_{i=1}^{N}\omega_i + \sum_{j=1}^{M}\omega_j\right)/(N+M)$$

$$\Delta V_i = k_{iw}\delta_i{}' = k_{iw}\frac{\omega_i - \omega_{\text{ave}}}{s}. \tag{15}$$

Equation (15) enables in each GFLC of the MG at the transient state and it does not influence the steady-state operation point for the MG. The feasibility of the proposed method will be verified in Section IV.

IV. Validations

To validate the theoretical analysis, hardware-in-loop experiment test rig is performed with OPAL-RT OP 5700 for the studied MG in Fig. 1. Fig. 7 shows the experimental setup and Table II lists the parameters. The circuit diagram is implemented by RT-Lab simulator and the control algorithms are programed with DSP28335. Since the perturbations of power angle and frequency eventually occur no matter what kind of large disturbances (short circuit fault, load switching, and voltage dropping) [5], the power angle and frequency after disturbance are directly set to test whether the system can recover to stable operation.

Fig. 8(a)–(c) presents the transient response of the MG under different disturbances with $\omega_c = 800$ Hz. When setting (x_1, x_2) after disturbance at (-1, 0), MG can return to the initial equilibrium point. When (x_1, x_2) after disturbance is at (-2, 0) which is the edge of the estimated DOA, the MG is finally stable after several oscillations. However, after the MG encounters a large disturbance at (-2.3, 0), the power angle and the angular frequency of GFLC diverge, which eventually leads to instability. Hence, the results confirm the effectiveness of the estimated ROA with current loop.

Since (-2.3, 0) is outside the estimated DOA with current loop but inside the estimated DOA without current loop, the instability of the MG also validates the overestimation caused by neglecting the dynamics of current controller.

Fig. 8(d) presents the transient response of the MG with $\omega_c = 500$ Hz. Assuming that (x_1, x_2) is at (-2, 0) after disturbance, the MG loses stability with increasing power angle and frequency of GFLC. The comparison with Fig. 8(b) verifies

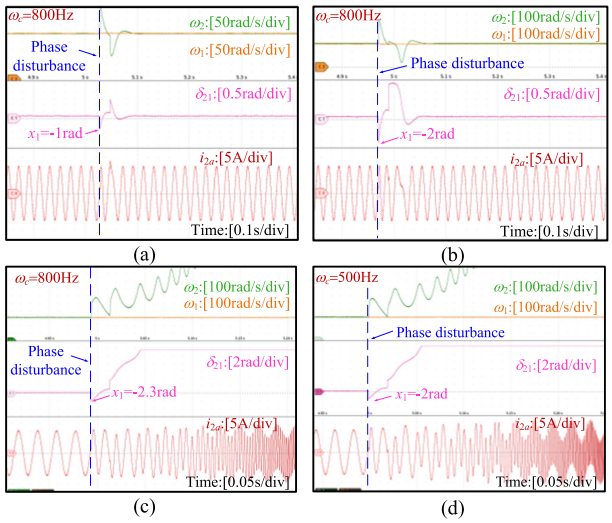

Fig. 8. Transient response of the MG with different (x_1, x_2) after disturbance (a) at (-1, 0) with $\omega_c = 800$ Hz, (b) at (-2, 0) with $\omega_c = 800$ Hz, (c) at (-2.3, 0) with $\omega_c = 800$ Hz, andE (d) at (-2, 0) with $\omega_c = 500$ Hz.

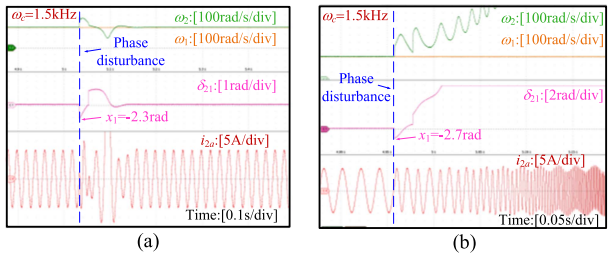

Fig. 9. Transient response of the MG with different (x_1, x_2) after disturbance (a) at (-2.3, 0) with $\omega_c = 1.5$ kHz and (b) at (-2.7, 0) with $\omega_c = 1.5$ kHz.

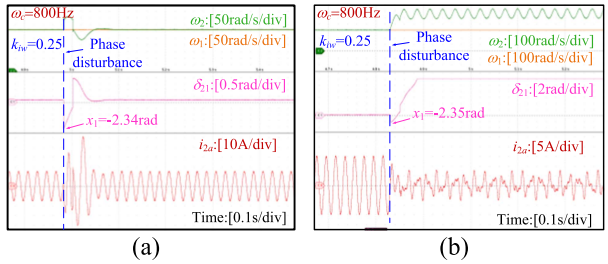

Fig. 10. Transient response of the MG with the proposed method. (a) (x_1, x_2) at (-2.34, 0). (b) (x_1, x_2) at (-2.35, 0).

that current controller with low dynamics has negative impact on the transient stability.

Fig. 9 presents the transient response of the MG with $\omega_c = 1.5$ kHz. The MG with (x_1, x_2) at (-2.3, 0) after disturbance can be stable while it loses stability when (x_1, x_2) is set as (-2.7, 0) after disturbance. The comparison with lower boundary of the estimated DOA without current loop validates that high frequency current controller also has obvious influence on transient stability margin, which is consistent with theoretical analysis in Figs. 3 and 4.

Fig. 10 presents the transient response of the MG with the proposed method. It can be observed that -2.34 rad is the lower

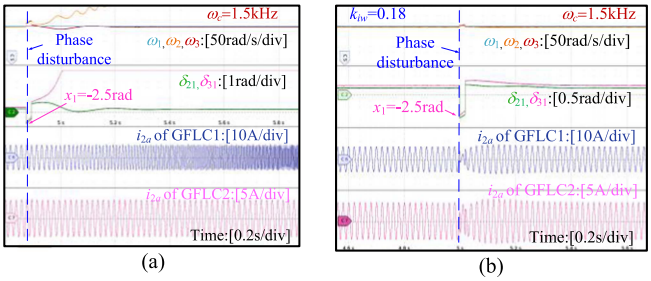

Fig. 11. Transient response of the MG with one GFMC and two GFLCs. (a) Without the proposed method; and (b) with the proposed method.

boundary of x_1 when k_{iw} is set as 0.25. Compared with Fig. 8, the results show that the stability can be enhanced by the proposed method. In addition, the relative error of lower boundary of x_1 can be reduced to 30%, which is consistent with parameter design guideline in Fig. 6(b).

Fig. 11 preliminarily tests the effectiveness of the proposed method for MG with one GFMC and two GFLCs. The reference currents $I_{d\text{ref}}$ for GFLC1 and GFLC2 are 20 and 15 A, respectively. The resistive load R_{load} is 4 Ω. Other parameters are the same with that in Table II. As depicted in Fig. 11, the phase stability of the MG can be ensured with the phase compensation method.

V. Conclusion and Future Work

In this letter, the influence of current controller on transient stability prediction of an island MG is studied. The main findings of this letter can be summarized as follows.

1) Neglecting dynamics of current controller can result in wrong prediction on transient stability margins.
2) The overestimation on angle stability boundary is more severe when dynamics of current controller is disregarded, even for high frequency current controller.
3) A stability-enhanced method by integrating phase compensation into current controller is proposed to improve the accuracy of transient stability assessment when ignoring dynamics of current controller.

This letter is limited in the scalability analysis of the transient stability estimation method and the proposed stability-enhanced method on large-scale MG with more GFLCs and GFMCs. More comprehensive studies regarding the scalability challenge would be conducted in future work. Additionally, how to assign the number of GFLCs and GFMCs in the MG for better transient stability is also worth for exploration.

References

[1] P. Alinaghi Hosseinabadi, S. Mekhilef, H. R. Pota, and M. Kermadi, "Chattering-free fixed-time robust sliding mode controller for grid-connected inverters under parameter variations," *IEEE J. Emerg. Sel. Topics Power Electron.*, vol. 12, no. 1, pp. 579–592, Feb. 2024.

[2] S. Zheng, K. Liao, J. Yang, and Z. He, "Optimal scheduling of distribution network with autonomous microgrids: Frequency security constraints and uncertainties," *IEEE Trans. Sustain. Energy*, vol. 14, no. 1, pp. 613–629, Jan. 2023.

[3] S. I. Habibi and A. Bidram, "Unfalsified switching adaptive voltage control for islanded microgrids," *IEEE Trans. Power Syst.*, vol. 37, no. 5, pp. 3394–3407, Sep. 2022.

[4] X. Xiong, C. Wu, P. Cheng, and F. Blaabjerg, "An optimal damping design of virtual synchronous generators for transient stability enhancement," *IEEE Trans. Power Electron.*, vol. 36, no. 10, pp. 11026–11030, Oct. 2021.

[5] Y. Tang, Z. Tian, X. Zha, X. Li, M. Huang, and J. Sun, "An improved equal area criterion for transient stability analysis of converter-based microgrid considering nonlinear damping effect," *IEEE Trans. Power Electron.*, vol. 37, no. 9, pp. 11272–11284, Sep. 2022.

[6] W. W. Weaver, R. D. Robinett, D. G. Wilson, and R. C. Matthews, "Metastability of pulse power loads using the Hamiltonian surface shaping method," *IEEE Trans. Energy Convers.*, vol. 32, no. 2, pp. 820–828, Jun. 2017.

[7] F. Chang, X. Cui, M. Wang, and W. Su, "Region of attraction estimation for DC microgrids with constant power loads using potential theory," *IEEE Trans. Smart Grid*, vol. 12, no. 5, pp. 3793–3808, Sep. 2021.

[8] B. Severino and K. Strunz, "Enhancing transient stability of DC microgrid by enlarging the region of attraction through nonlinear polynomial droop control," *IEEE Trans. Circuits Syst. I, Reg. Papers*, vol. 66, no. 11, pp. 4388–4401, Nov. 2019.

[9] Z. Duan, Y. Meng, Y. Duan, H. Zhang, X. Wang, and X. Wang, "Large-signal stability analysis and enhancement of modular multilevel matrix converter under power fluctuation based on T-S fuzzy model theory," *IEEE Trans. Power Electron.*, vol. 38, no. 11, pp. 14601–14613, Nov. 2023.

[10] Z. Tian et al., "Transient synchronization stability of an islanded AC microgrid considering interactions between grid-forming and grid-following converters," *IEEE J. Emerg. Sel. Topics Power Electron.*, vol. 11, no. 4, pp. 4463–4476, Aug. 2023.

[11] W. Du, J. Zhang, Y. Zhang, and Z. Qian, "Stability criterion for cascaded system with constant power load," *IEEE Trans. Power Electron.*, vol. 28, no. 4, pp. 1843–1851, Apr. 2013.

[12] J. Jiang et al., "A conservatism-free large signal stability analysis method for DC microgrid based on mixed potential theory," *IEEE Trans. Power Electron*, vol. 34, no. 11, pp. 11342–11351, Nov. 2019.

[13] Q. Song, J. Chen, K. H. Loo, J. Chen, and P. Chen, "Large-signal stability analysis of two-stage cascaded DC/DC converter systems using sum-of-squares programming," *IEEE Trans. Power Electron.*, vol. 39, no. 2, pp. 2076–2085, Feb. 2024.

[14] Y. Du, Y. Men, L. Ding, and X. Lu, "Large-signal stability analysis for inverter-based dynamic microgrids reconfiguration," *IEEE Trans. Smart Grid*, vol. 14, no. 2, pp. 836–852, Mar. 2023.

[15] M. H. Roos, P. H. Nguyen, J. Morren, and J. G. Slootweg, "Stability analysis of microgrid islanding transients based on interconnected dissipative subsystems," *IEEE Trans. Smart Grid*, vol. 12, no. 6, pp. 4655–4667, Nov. 2021.

[16] H. Cheng, Z. Shuai, C. Shen, X. Liu, Z. Li, and Z. J. Shen, "Transient angle stability of paralleled synchronous and virtual synchronous generators in islanded microgrids," *IEEE Trans. Power Electron.*, vol. 35, no. 8, pp. 8751–8765, Aug. 2020.

[17] M. Kabalan, P. Singh, and D. Niebur, "A design and optimization tool for inverter-based microgrids using large-signal nonlinear analysis," *IEEE Trans. Smart Grid*, vol. 10, no. 4, pp. 4566–4576, Jul. 2019.

[18] Y. Li et al., "PLL synchronization stability analysis of MMC-connected wind farms under high-impedance AC faults," *IEEE Trans. Power Syst.*, vol. 36, no. 3, pp. 2251–2261, May 2021.

[19] L. Meng, T. Dragicevic, J. Roldán-Pérez, J. C. Vasquez, and J. M. Guerrero, "Modeling and sensitivity study of consensus algorithm-based distributed hierarchical control for DC microgrids," *IEEE Trans. Smart Grid*, vol. 7, no. 3, pp. 1504–1515, May 2016.